Title
A MODULATED MOLECULAR BEAM STUDY OF THE MECHANISM OF THE H2-D2 EXCHANGE REACTION ON Pt(lll) AND Pt(332) CRYSTAL SURFACES

Author
Salmeron, M.

Publication Date
1978-05-01

Submitted to Journal of Chemical Physics

LBL-7627
Preprint

c.2

A MODULATED MOLECULAR BEAM STUDY OF THE MECHANISM OF THE H_2-D_2 EXCHANGE REACTION ON Pt(111) AND Pt(332) CRYSTAL SURFACES

M. Salmerón, R. J. Gale, and G. A. Somorjai

May 10, 1978

Prepared for the U. S. Department of Energy
under Contract W-7405-ENG-48

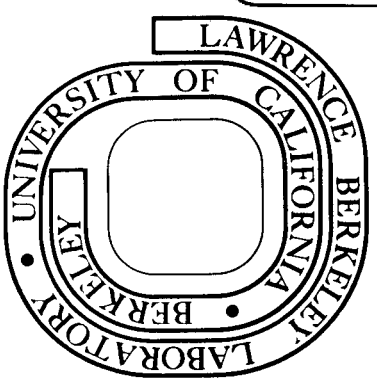

LBL-7627

c.2

DISCLAIMER

LBL 7627

A MODULATED MOLECULAR BEAM STUDY OF THE MECHANISM OF THE H_2-D_2 EXCHANGE REACTION ON Pt(111) AND Pt(332) CRYSTAL SURFACES

by

M. Salmerón*, R. J. Gale and G. A. Somorjai

Materials and Molecular Research Division, Lawrence Berkeley Laboratory, and Department of Chemistry, University of California, Berkeley, California 94720

Abstract

The interaction of hydrogen with platinum has been studied by the exchange reaction $H_2+D_2=2HD$ on two crystal surfaces, a flat(111) and a stepped(332) (in step notation, (S)-[6(111)x(111)]). The adsorption of hydrogen appears to be an activated process on the Pt(111) surface, with a barrier height of ~0.5-1.5 kcal/mole. On the Pt(332) surface, the adsorption of hydrogen requires no activation energy. The recombination of H and D atoms to form HD follows, on both surfaces, a parallel mechanism with one of the branches operative in the entire temperature range studied, 25-800°C. This branch has an activation energy and pseudo-first-order preexponential of E_1=13.0±0.4 kcal/mole and A_1=(8±3)x10^4sec^{-1} for the Pt(332) surface and E_1=15.6±0.5 kcal/mole and A_1=(2.7±1)x10^5sec^{-1} for the Pt(111) surface. For temperatures above ~300°C, the second branch is observed, but the values of the

---

* Permanent Address: Instituto de Física del Estado Sólido (C.S.I.C.) and Departamento de Física Fundamental, Universidad Autónoma de Madrid, Canto Blanco (Madrid) Spain.

preexponential factors and activation energies could not be uniquely determined for either of the two crystals. Below ~300°C a third process appears in series with the first branch. The scatter in the data at low temperatures due to the small signal amplitude prevents accurate determination of the rate constants for this reaction step.

1. Introduction

Although the interaction of hydrogen with platinum has been extensively studied over the past twenty years, it is not well understood on the atomic scale. However, it has been established that the presence of monatomic steps in a (111) surface enhances the adsorption and dissociation of hydrogen relative to the flat surface (1-7). Our recent study (6, 7) of the dependence of H_2-D_2 exchange on the angle of incidence of the reactants has shown that the region of initial impact on a stepped surface determines the probability of dissociative adsorption. The most favorable region for hydrogen adsorption was found to be associated with the inner corner of the step structure.

Very little is known about the next step in the reaction process, i.e., the recombination of adsorbed atoms to form H_2, D_2 or HD and subsequent desorption as molecules. The kinetics of this process can be studied by thermal desorption, isotopic exchange, and particularly by molecular beam reactive scattering. In such experiments, the reaction is studied far from equilibrium, a necessary condition for obtaining kinetic information.

Only the molecular beam technique allows complete definition of the reaction conditions. A molecular beam of the reactants impinges on the well characterized surface of the catalyst, which is maintained in ultra high vacuum conditions (UHV). The intensity of the beam (or equivalent reactant pressure), its velocity (or temperature) and angle of incidence can be specified. In conventional isotropic experiments, the last two parameters are not generally variable.

Another important advantage of the molecular beam technique is the possibility of modulating the intensity of the beam. Such modulation increases the signal to noise ratio as a consequence of using phase sensitive lock-in detection. Also, time (or frequency) is introduced as a new variable in the experiment. The response of the system to the periodic pulses of reactants consists, for each harmonic of the partial pressure of the reaction products, of an amplitude r, and a phase lag ϕ, relative to that of the incident reactants. The response of the system will be determined by the relation between the modulation period τ and the reaction time t, which depends on the temperature of the crystal. When $\tau<t$, the surface reaction from the previous pulse is not yet completed when the next pulse of reactants strikes the surface. The system can not follow the rapid changes of pressure of the reactants. Under such conditions, the amplitude of the products, r, is small and the phase lag, ϕ, is large. When $\tau>t$, the surface reaction follows the variations of beam intensity and consequently the amplitude of the product signal is large and its phase lag small. In fact, it is possible to study the kinetics of a surface reaction by measuring the amplitude and phase lag of the reaction products as a function of surface temperature and modulation frequency. From the shape of the curves, r and $\tan\phi$ vs. T (or 1/T, where T is the crystal temperature), we can also determine whether the reaction rate is controlled by a single step (for example, desorption), two parallel steps with different rate constants (branched reaction) or two steps connected in series, etc. The behavior of r and ϕ vs. the experimental parameters, crystal temperature, modulation frequency and beam pressure, has been analyzed in detail for

many typical surface reaction models, and hence, we shall not try to develop this subject here. The interested reader is directed to excellent reviews on that subject (8-10). However, the shape of the Arrhenius plots of the amplitude and tanϕ for the processes that are relevant to the present work are displayed in Fig. 1. In Fig. 1(A) and (B), the variation of r and tanϕ for a single step process are plotted. Fig. 1(C) and (D) show the form of the tanϕ curves for parallel and series processes, respectively.

We have used the modulated beam technique to study the $H_2 + D_2 = 2HD$ reaction on two platinum surfaces, a flat (111) and a stepped (332) surface. The stepped surface consists of a periodic arrangement of terraces of (111) orientation, separated by monatomic steps also of the (111) orientation. This is, in step notation, the Pt (S)-[6(111)x(111)]. From the shape of the experimental r and tanϕ curves, it appears, by comparison with the theoretical curves shown in Fig. 1, that the reaction is branched for temperatures above $\sim$300°C, on both Pt(111) and Pt(332) crystals. Another slow reaction step appears at lower temperatures, which is connected in series, also for both crystal surfaces. This type of detailed kinetic information can only be obtained by molecular beam relaxation methods, and is not available using more conventional techniques.

2. Experimental

The experiments were performed in a UHV chamber equipped with low energy electron diffraction (LEED) and Auger electron spectroscopy (AES), which has previously been described in detail (2,7).

For this study, a mixture of H_2 and D_2 was used to form a beam with an H_2/D_2 ratio of $\sim$5:1 to $\sim$12:1, with an average intensity on the order

of 10^{13}-10^{14} molecules per cm^2 second at the crystal with the chopper on.

The gaseous reactants and products were monitored using a rotatable quadrupole mass spectrometer and phase sensitive lock-in detection. The two modes of detection, differential and integral, have been discussed in detail in a recent publication (7), and therefore will only be briefly described here.

In the differential mode, the mass spectrometer is positioned at a certain scattering angle from the surface normal. The signal detected is composed of two contributions for a given mass number. One part is due to the species directly emitted from the surface at that particular angle (with an angular aperture of $\sim 5^{\circ}$). The second contribution is from the modulated partial pressure of the species being analyzed, which is due to its finite residence time in the UHV chamber before being pumped away. This second contribution must be measured independently and subtracted from the total signal to obtain the first one, or the true differential signal. The phase and amplitude of the differential product signal is then referenced to the direct beam of reactants. We have used this method of detection, for example, to obtain the angular distribution of the emitted species H_2, D_2 and HD (in the plane of incidence). To obtain the total amount of HD emitted from the surface, the true differential signal must be integrated over all angles and that requires knowledge of the angular distributions at all angles of emission.

In the second method, the integral mode, only the modulated partial pressure of the reactants and products is measured. For the products, this is accomplished by positioning the mass spectrometer behind the crystal such that no species directly emitted from the surface can enter

the ionizer. The modulated partial pressure of the reactants can be measured in two ways, which give the same result. The manipulator can be rotated such that the beam strikes the back of the crystal support or the flag can be placed in the beam line. In each case, the beam is scattered from a nonreactive surface as established by monitoring the HD partial pressure. The phase and amplitude of the product signal is then referenced to that of the reactant signal. All of the results of phase and amplitude reported in this study have been obtained using this method. This method has several advantages. (i) The signal measured is proportional to the total amount of HD emitted (i.e., integrated over all emission angles). (ii) The measured signal does not contain any other contribution that has to be subtracted, as in the differential method, thus reducing errors.

The temperature of the Pt crystals was measured with a chromel-alumel thermocouple spot-welded to the edge of each crystal.

The crystals, Pt(332) and Pt(111), were examined with LEED and AES prior to and after each experiment. Most of the results reported here correspond to clean crystals as established by AES. The orientation of the surfaces, indicated by the LEED patterns, showed the expected periodicity for the stepped Pt (S)-[6(111)x(111)] and flat Pt(111).

Argon ion sputtering and/or heating the crystals at 600-800^{o}C in 10^{-7} to 10^{-6} torr of oxygen proved effective in producing surfaces free from impurities detectable by AES.

The procedure for obtaining the data shown in Figs. 3-8 was to heat the crystal up to $\sim$1,000^{o}C and allow it to cool at a fixed frequency of modulation while monitoring the HD partial pressure.

3. Results

3.1. Influence of Uncontrolled Surface Defects on the Production of HD

That the presence of surface defects is effective in enhancing the reactivity of the Pt surface is dramatically illustrated in Fig. 2. This figure shows the production of HD as a function of the position of the reactant beam on the surface of a Pt crystal that has been subjected to three different types of mechanical polishing and chemical etching. The two upper curves correspond to crystals with different degrees of edge damage. The three crystals, however, exhibited the same LEED pattern across the surface. These results demonstrate another advantage of using molecular beams. The area of the surface free from damage can be located to perform the experiment and in any case allows a check of the importance of edge effects.

3.2. H_2-D_2 Exchange on the Stepped Pt(332) Crystal Surface

In Figs. 3 and 4 the amplitude and the phase of the HD product signal are plotted as a function of the reciprocal surface temperature (r and tanϕ vs. $10^3/T$) for the stepped platinum crystal surface at various beam modulation frequencies. In these experiments, the angle of incidence of the mixed H_2-D_2 beam was $\theta = 45^o$ with respect to the macroscopic surface normal. The step orientation is such that the beam strikes perpendicular to the step edges, into the open side ("upstairs" direction), as depicted in the insert in Figs. 3 and 4. The different runs correspond to experiments performed on different days and hence with different incident beam intensities and composition. The shape of the curves is identical when the beam strikes from the opposite direction ("downstairs" direction),

but the amplitude is almost a factor of 2 smaller, as we have previously reported (6, 7). There are three reaction regions distinguishable in Fig. 4 that correspond to temperatures above 300°C, between 200 and 100°C and below 100°C. In the high-temperature region the phase data show considerable scatter due to the small phase lags which must be obtained by subtracting two finite phase angles corresponding to the incident D_2 (or H_2) and the reaction product HD.

Between 300°C and 200°C there is an inflection in the phase lag curve. Below 200°C, the experimental points follow a straight line down to the lowest temperatures, where they bend up when ϕ becomes larger than 90°. At this point $\tan\phi$ becomes very large and then changes sign. These points have been represented with filled circles and squares in Fig. 4. As can be seen in this figure, the temperature at $\phi = 90^{\circ}$ depends on the frequency of modulation and is lower at the low frequencies. The scatter in the data is large at the lower temperatures because the amplitude of the signal has become very small (see Fig. 3).

These data were obtained starting with the crystal at high temperature and cooling it to ~100°C. Below this temperature the cooling rate was very slow, controlled by the thermal conductivity of the crystal support. The experiments to obtain each curve took from 30 to 60 minutes. The reproducibility of the results was excellent from one day to another except for small vertical displacements in the curves of Fig. 4 of up to 10°. This is related to the difficulty of reproducing a beam of the same intensity and composition. It should be noted that for a second-order reaction, the phase lag depends on the reactant pressure (9).

At the very high temperatures (T>800°C), there is a small but clearly reproducible decrease in the amplitude of the HD signal, accompanied by an increase in the phase lag. This result is just detectable in Fig. 3. This could be attributed to an increase in the solubility of H_2 in Pt, above 800°C, that would result in a decrease in the concentration of H-atoms at the surface. The increase in the phase lag is also consistent with the appearance of a diffusion-controlled step in the reaction (8). We shall not consider this process, however, in this study.

3.3. H_2-D_2 Exchange on the Pt(111) Crystal Surface

The reactive scattering data for this crystal were obtained with the mixed H_2-D_2 beam incident normal to the surface ($\theta = 0^o$). The corresponding amplitude and phase data as a function of the reciprocal crystal temperature are shown in Figs. 5 and 6. Most of the remarks made in the case of reactive scattering from the Pt(332) can be repeated here. The shape of the tanϕ vs. 1/T curves is very similar to that from the Pt(332) crystal. The straight line region below 300°C, however, has a somewhat steeper slope. Another important difference when compared with the stepped crystal is the slope of the amplitude curves at high temperatures. This result can only be explained, in our opinion, by an activation barrier for adsorption, which is absent on the Pt(332) crystal. We shall comment on this point in more detail in the discussion section.

There is a hysteresis in the amplitude and phase lag data between cooling and heating cycles. An example of this effect on the phase lag is shown in Fig. 7 for Pt(111). We believe that this hysteresis is associated with the presence of unwanted adsorbates when starting from room

temperature. The impurities that were adsorbed during the long exposure time at low temperature are progressively desorbed with the increasing temperature. The product amplitude, for example, does not reach (in many cases) its full value (i.e., the value found in the cooling cycle) until the temperature reaches 600°C. Above this temperature the hysteresis disappears completely. For this reason, we believe that the data obtained during the cooling cycle are more reliable and we have used them exclusively in the discussion of the reaction. Another observation that supports this idea is the reproducibility of the results, which is very good for the cooling cycles, but only fair for the heating ones.

3.4. The Effect of Silicon Segregation on the Reactivity of the Pt(111) Crystal

For some of the Pt(111) crystals used, segregation of silicon to the surface was observed during the cooling of the crystal from ~1,000°C to room temperature. The exchange reaction exhibits a decrease in the amplitude of the HD signal, as shown in Fig. 8, without, however, any dramatic change in the phase lag. We interpret this result as due to the presence of silicon on the surface that blocks a fraction of the adsorption sites but does not participate in the reaction in any other way.

3.5. Angular Distribution of HD from the Stepped Pt(332) Surface

In Fig. 9, the angular distribution of the reaction product HD from the Pt(332) crystal, measured in the plane defined by the reactant beam and the macroscopic surface normal, is presented, for two azimuthal

angles. As shown in the insert in Fig. 9, for $\Phi = 90^{o}$, the beam impinges perpendicular to the open side of the step edges. For $\Phi = 0^{o}$, the projection of the incident beam on the surface is parallel to the step edges. In both cases, the angle of incidence is $\theta = 45^{o}$, relative to the macroscopic surface normal. The observed distribution for both azimuthal angles is closer to a $\cos^{2}\Omega$ dependence than to $\cos\Omega$, as indicated by the solid and dotted lines, respectively, in Fig. 9.

3.6. Dependence of the Reaction Probability on the Angle of Incidence on the Stepped Pt(332) Surface

In a preceding study (6, 7), we have shown that the production of HD depends markedly on the angle of incidence of the reactants on a stepped platinum surface. The reactivity was found to be highest when the beam strikes the open side of the step edges. In that study the temperature of the crystal was fixed at 800°C. The question arises as to whether this angular effect is also present at lower temperatures. Therefore, we have performed a series of experiments for crystal temperatures down to 200°C. As can be seen in Fig. 10, the angular dependence of the reaction probability is still clearly visible. For lower crystal temperatures, the production of HD showed a continuous decrease with time, probably due to surface contamination from the ambient. The production of HD as a function of the angle of incidence of the reactants is shown in Fig. 11 for a crystal temperature of 100°C. Although a decrease in the amplitude with time is clearly apparent in Fig. 11, it seems that the anisotropy observed at higher temperatures tends to disappear. This important result needs more careful investigation, however.

4. Discussion

In the following discussion we shall assume that the reaction $H_2+D_2=2HD$ is second order. This means that the reaction involves the facile breaking of H-H bonds at the surface, followed by the recombination of the adsorbed H and D atoms to form HD as the rate-limiting step. This assumption is based on previous observations by other authors (3-5, 11, 12) as well as on the fact that the measured phase lag depends on the pressure of the reactant beam. Although we have not made a systematic study of this dependence, it has been observed when comparing the tanϕ data from different experiments. The curves obtained at different beam pressures and composition require a vertical displacement to coincide, of the order of $\sim \pm 5^{o}$ in the phase angle for our range of variation in beam pressure and composition.

The fact that the shape of the tanϕ, curves is similar for the two platinum crystals with different surface structure is a clear indication of the similarity of the reaction mechanism operating for both the flat and the stepped crystals. This similarity is particularly striking in the following features. (i) The appearance of a bump at $10^3/T \simeq 1.9$, which separates a straight line region at low temperatures and a steeper region at higher temperatures. (ii) The fact that although the slope of these low-temperature regions is different for the two crystals, the curves bend up and tanϕ eventually becomes negative ($\phi > 90^{o}$), for both surfaces. This bending is more apparent at high modulation frequencies, where the straight line region almost completely distorted. In view of the shapes of the tanϕ curves shown in Fig. 1, we conclude that, in both crystals, the recombination mechanism consists of two reaction steps acting in

parallel at high temperatures (T>300°C), and a series reaction at the lowest temperatures. In order to work out a simple model for the H_2-D_2 exchange kinetics the following simplifying assumptions will be made. (i) We assume that the diffusion of molecularly adsorbed H_2 and D_2 on the surface may be neglected. In the case of the Pt(332) crystal, this assumption is based on the angular dependence displayed in Fig. 10 and on studies described in references 6 and 7. Since the reactivity appears to be highest when the mixed H_2-D_2 beam strikes the open side of the step edges, at least for surface temperatures above 200°C, we can conclude that the molecular diffusion length is not larger than the terrace width $\sim$ 15Å. (ii) Isotope effects in the process of adsorption and dissociation of H_2 and D_2 and in the diffusion and recombination of H and D atoms are ignored. Although this may not be appropriate it will not change greatly the magnitude of the preexponential factors. In any case, the uncertainty in the absolute beam intensity would contribute even larger errors in the measured preexponential factors. (iii) The amount of H_2, HD, and D_2 formed by recombination of H and D atoms in the surface with concentrations n_H and n_D, is proportional to n_H^2, $2n_Hn_D$, and n_D^2, respectively. In the absence of isotope effects, the relative amounts of H and D on the surface, n_H/n_D, is equal to the corresponding ratio in the beam, H_2/D_2. Thus, we can write, in steady-state conditions (at zero modulation frequency, f), the rate of HD desorption as

$$R_{HD} = 2\sigma R_{H_2} \cdot R_{D_2} / (R_{H_2} + R_{D_2}) \qquad (1)$$

or

$$r \equiv 2\sigma = \frac{R_{HD}}{R_{D_2}} \cdot (1 + R_{D_2}/R_{H_2}) \qquad (2)$$

where σ is the sticking coefficient for dissociative adsorption and R_{H_2} and R_{D_2} the number of molecules (H_2 or D_2) from the beam striking the crystal, per unit area and unit time. This result means that for an H_2/D_2 ratio much greater than 1, any D_2 molecule that is adsorbed dissociatively must give rise to two HD molecules. Under these conditions, the ratio R_{HD}/R_{D_2} should be equal to twice the sticking coefficient for dissociative adsorption 2σ. This value of r is the high-temperature value of the relative amplitude of the HD signal for all of the models discussed in the following sections. Under our experimental conditions, the factor $1+R_{D_2}/R_{H_2}$ has a value between 1.1 and 1.2. (iv) On the basis of the above considerations, in the discussion of the reaction models for the H_2-D_2 exchange will be treated as an H recombination process and we shall omit any distinction between H and D.

4.1. Reaction Models

In order to extract the kinetic parameters from our experimental data, the theoretical reaction model that best fits the data must be found. It is, of course, of prime interest to find the simplest model that is physically reasonable. We have found that a single step second-order reaction, even with a coverage dependent adsorption probability, activation energy or preexponential factor, does not explain our experimental results. A branched mechanism, including a series process at low temperatures, yields the best fit to our data. The model calculations are described in detail below.

(a) Second-order reaction. Although the shape of the tanϕ curves does not seem to correspond to that of a simple recombination reaction (compare Figs. 4 and 6 with Fig. 1B), there appear to be conditions that may cause significant deviations of the Arrhenius plot of tanϕ from a straight line. In a detailed analysis of the exact and approximate solutions of the mass balance equations for nonlinear surface reactions, Olander et al. (10) point out that bumps or maxima in the ϕ (or tanϕ) vs. 1/T curves could appear due to the dependence of σ (the sticking coefficient) or k (the rate constant), on surface coverage. The mass balance equation for the concentration of surface atoms, n, when there is only one recombination step is:

$$\frac{dn}{dt} = 2\sigma \cdot g(\theta) \cdot I(t) - 2kn^2 \qquad (3)$$

where we have explicitly separated the coverage dependent occupation factor $g(\theta)$, from the bare surface sticking coefficient σ. I(t) is the number of molecules colliding with the surface per unit area and unit time at time t. The rate constant k is written in the usual Arrhenius form $A_o \cdot \exp(-E/RT)$, where A_o is the preexponential factor and E the activation energy.

We have solved the above equations for $g(\theta) = (1-\theta)^2$ by using the approximate method of Olander et al. (10). The periodic function I(t) is approximated by:

$$I(t) = I_o + I_1 \cdot \exp(i\omega t) \qquad (4)$$

where $\omega = 2\pi f$, f = frequency of modulation, I_o is the dc term of the Fourier expansion of I(t) plus any background contribution. The

coverage dependent term $g(\theta)$ is approximated by:

$$g(\theta) = g(\bar{\theta}) + \left.\frac{dg}{d\theta}\right|_{\theta=\bar{\theta}} \cdot (\theta-\bar{\theta}) \qquad (5)$$

where

$$\bar{\theta} = \frac{\omega}{2\pi} \cdot \int_0^{2\pi/\omega} \theta(t) \cdot dt$$

is the mean coverage during one cycle.

If we first assume k to be independent of θ, Eq. (3) can be solved exactly for a square wave gating function. After obtaining $\bar{\theta}$, the Eqs. (4) and (5) are used to solve Eq. (3) and then compute the first harmonic of the desorption rate $k.n^2$. The result for $\tan\phi$ does not show any bump or any other feature comparable to that observed experimentally.

The next step was to introduce a coverage dependent activation energy and preexponential. These calculations were performed separately in two steps. First we have assumed a coverage dependent activation energy together with a coverage dependent sticking coefficient through $g(\theta)=(1-\theta)^2$. The dependence of E on θ was introduced empirically as $E=E_o-B \cdot \theta^2$. This expression may represent approximately the results of Christmann et al. (4), who effectively found that the binding energy of H on Pt(111) decreases with coverage when $\theta \gtrsim 0.5$. In another case, we have used a rapidly decreasing function, $E(\theta)=E_o \cdot \exp(-\theta/\theta_o)$. In both cases, by appropriately choosing values of the parameters B and θ_o, the qualitative behavior of the calculated $\tan\phi$ vs. $1/T$ curves was similar to the experimental results. However, the calculated values of $\tan\phi$ were at least two orders of magnitude greater than the experimental values at low temperatures. This difference was not very sensitive to the analytical

form of $E(\theta)$. The reason for this discrepancy is that these models imply that at the transition temperature (between 300° and 200°C in our case), the coverage becomes very large (i.e., near unity). Under these conditions the calculated phase lag approaches 90°. Therefore, our experimental results can not be explained by this type of model. Although this does not mean that the rate constant k cannot depend on θ, that dependence is not responsible for the observed shape of the r and $\tan\phi$ vs. 1/T curves. The effect of a coverage dependent preexponential in the rate constant expansion, i.e., $k = A(\theta) \cdot \exp(-E/RT)$ has also been examined. However, this type of model does not fit our experimental data either.

We are led then to conclude that a simple reaction step, even with coverage dependent sticking coefficient and rate constant, is not sufficient to explain our experimental data. In the following sections, we shall analyze the parallel and series reaction mechanisms suggested by the forms of the model curves of Fig. 1 to fit our data.

(b) Parallel reaction models. We have studied two models (I and II) involving parallel reaction steps. These are depicted schematically by the following schemes:

I. $2H_2(gas) \begin{cases} \xrightarrow{p.\sigma} 2H(ads.)_2 \xrightarrow{k_2} H_2(ads.) \longrightarrow H_2(gas) \\ \xrightarrow{(1-p).\sigma} 2H(ads.)_1 \xrightarrow{k_1} H_2(ads.) \longrightarrow H_2(gas) \end{cases}$

II. $2H_2(gas) \begin{cases} \xrightarrow{p.\sigma} 2H(ads.)_2 \xrightarrow{k_2} 2H(ads.)_1 \\ \xrightarrow{(1-p).\sigma} 2H(ads.)_1 \xrightarrow{k_1} H_2(ads.) \longrightarrow H_2(gas) \end{cases}$

In model I, two independent recombination processes may occur simultaneously at sites 1 and 2, with different rate constants k_1 and k_2. In each branch, the rate-limiting step is a second-order recombination. The parameter p is the branching ratio.

In model II, the rate-limiting step in branch 2 is the transfer of atoms to sites 1. It is, then, a first-order step. In this model, we have neglected the reverse transfer, i.e., from sites 1 to 2. This approximation is justified since at low temperatures ($T<200$-300^oC), the sites 2 are completely covered (a result confirmed a posteriori), and at high temperatures the coverage of sites 1 is too small for any significant transfer of adsorbates to 2 (as compared with the contribution from the direct beam to the occupancy of sites 2).

If the values of the activation energies and preexponentials are sufficiently different in each branch, there will be temperature regions where only one branch will be active (low-temperature branch), or both branches will be active (low- and high-temperature branches). This is the case in our experiments and the bump at $10^3/T \simeq 1.9$ separates, in both models, the high- and low-temperature regions. By using the approximation (4), and taking $\bar{\theta}$ to be the dc term in the Fourier expansion of θ, we obtain the following expression for the amplitude, r, and phase lag, ϕ:

Model I

$$r \cdot \exp(-i\phi) = r_1 \cdot \exp(-i\phi_1) + r_2 \cdot \exp(-i\phi_2) \qquad (6)$$

where

$$\tan\phi_1 = \frac{\omega}{4\sqrt{\sigma(1-p)I_o k_1}} \qquad r_1 = \frac{2\sigma(1-p)}{\sqrt{1+\tan^2\phi_1}} \qquad (7)$$

and

$$\tan\phi_2 = \frac{\omega}{4\sqrt{\sigma p I_o k_2}} \qquad r_2 = \frac{2\sigma p(1-\theta_o)^2}{\sqrt{\left(\frac{1}{1-\theta_o}\right)^2 + \left(\frac{\omega}{4k_2 N_2 \theta_o}\right)^2}} \tag{8}$$

where I_o is the average number of molecules (beam plus background) striking the surface per unit area per unit time. θ_o is the mean coverage of type 2 sites and N_2 the number of sites 2 per unit area.

Model II

$$r \cdot \exp(-i\phi) = r_1 \cdot \exp(-i\phi_1) \cdot \left(1 + \frac{p}{(1-p)} \cdot r_2 \cdot \exp(-i\phi_2)\right) \tag{9}$$

where

$$\tan\phi_1 = \frac{\omega}{4\sqrt{\sigma(1-p) I_o k_1 + \left(\frac{k_1 k_2 N_2 \theta_o}{2}\right)}} \tag{10}$$

$$r_1 = \frac{2\sigma(1-p)}{\sqrt{1+\tan^2\phi_1}} \tag{11}$$

and

$$\tan\phi_2 = \frac{\omega}{k_2 + \left(\frac{4\sigma p I_o (1-\theta_o)}{N_2}\right)} \tag{12}$$

$$r_2 = \frac{(1-\theta_o)^2}{\sqrt{\left(1 + \frac{4\sigma p I_o (1-\theta_o)}{k_2 N_2}\right)^2 + \frac{\omega^2}{k_2^2}}} \tag{13}$$

A common feature of both models is their low-temperature branch. At low temperatures when branch 2 is no longer active ($k_2 \simeq 0$), both models give:

$$\tan\phi \simeq \frac{\omega}{4\sqrt{\sigma(1-p)A_1^0 I_0}} \cdot \exp(E_1/2RT) \equiv \frac{\pi f}{2A_1} \cdot \exp(E_1/2RT) \qquad (14)$$

where we have written explicitly the rate constant k_1 as $A_1^0 \cdot \exp(-E_1/RT)$. At low temperatures, the Arrhenius plot of $\tan\phi$ will be a straight line whose slope gives directly $E_1/2R$ and whose intercept at the origin gives $A_1 = \sqrt{\sigma(1-p)A_1^0 I_0}$, giving us A_1^0, the preexponential factor, provided the other parameters are known.

In the high-temperature limit, both models also give the same result for the amplitude: $r = 2\sigma$, since in both cases ϕ_1 and ϕ_2 become zero.

(c) Series reaction. As we have shown, the experimental phase lag for low temperatures and high frequencies becomes larger than 90^o, such that $\tan\phi$ becomes negative (see Figs. 4 and 6). This fact is an indication of the existence of another step at these low temperatures acting in series with branch 1 of the preceding models. Schematically this is depicted

$$H_2 \xrightarrow{\sigma} 2H(\text{ads.}1) \xrightarrow{k_1} H_2(\text{ads.}3) \xrightarrow{k_3} H_2(\text{gas})$$

or other similar processes. The phase lag in this model is:

$$\phi = \phi_1 + \phi_3 \qquad \tan\phi_1 = \frac{\omega}{k_1'} \qquad \tan\phi_3 = \frac{\omega}{k_3} \qquad (15)$$

where $k_1' = 4\sqrt{\sigma(1-p)I_0 k_1}$ for a second-order step.

We shall now discuss the application of these models to our data for each crystal separately.

4.2. The Stepped Pt(332) Crystal Surface

The values of the pseudo-first-order preexponential factor A_1 and activation energy E_1 corresponding to the low-temperature branch, have been measured directly from the curves of Fig. 4, for $10^3/T>1.9$. The average of the values obtained from various runs are: $E_1 = 13.0 \pm 0.4$ kcal/mole and $A_1 = (8 \pm 3) \times 10^4$ sec^{-1}.

For the estimated beam intensity of $I_o \simeq 10^{13}$-10^{14} molecules per cm^2 second, we obtain an estimate of A_1^o of 10^{-3}cm^2/sec. This value is in good agreement with what should be expected for a second-order surface reaction. According to the transition state theory the preexponential factor is given by: $(KT/h) \cdot Q^*/Q_H^2$, where Q^* is the partition function for the transition state, an H-H molecule, and Q_H the partition function for an adsorbed H-atom. Taking $Q^* = q_T^2 \cdot q_R$, q_T and q_R being the translational and rotational partition functions respectively, and $Q_H = q_T^2$, we obtain an order of magnitude estimate for A_1^o of 10^{-3}cm^2/sec. (13).

The value of σ is also obtained directly from the experimental data at the highest temperatures: $2\sigma = .6$ to $.7$, i.e., $\sigma \simeq .33 \pm .03$ at 45^o angle of incidence with the reactant beam striking the open side of the step edges.

The procedure to obtain the remaining constants, p, A_2^o and $E_2(k_2 = A_2^o \cdot \exp(-E_2/RT))$, was through least squares fitting Eqs. (6) - (13) to the experimental data at 50 Hz. This fitting procedure was performed for the two models of parallel reactions described above. Unfortunately, the scattering of the tanϕ data in the high-temperature region is such that the values of A_2^o and E_2 cannot be determined uniquely. We

have found that pairs of values related through $4 \cdot \log(\sqrt{\sigma p A_2^o I_o}) \simeq E_2$ (in kcal/mole and sec^{-1}) give fits of approximately the same quality. In fact, "good" values of E_2 range from 20 to 50 kcal/mole. The same is true for model II, where the pairs of A_2^o and E_2 values are related through $2 \cdot \log(A_2^o) \simeq E_2$. Since a second-order step implies a preexponential $A_2^o = 10^{-3}$ to 10^{-1}, the value of E_2 (in model I) should be of the order of 20 to 30 kcal/mole. In model II, since the rate-limiting step is first order, A_2^o must be of the order of 10^{11} to 10^{13} sec^{-1} and the corresponding values of E_2 must again be between 20 and 30 kcal/mole. In both models, the "best" branching ratio, p, is $\sim 1/4$. With the values of A_1 and E_1 measured for the low-temperature branch and the values $A_2^o = 10^{12}$ sec^{-1}, $E_2 = 25$ kcal/mole (model II), we obtain the continuous curves shown in Figs. 3 and 4, computed with Eqs. (9) - (13). The curves obtained with model I are very similar as can be seen in the broken curve of Fig. 4 around $10^3/T = 1.8$. This curve has been computed with Eqs. (6) - (8), with $A_2^o = 10^{-1}$ cm^2/sec and $E_2 = 25$ kcal/mole, for f = 50 Hz.

As can be seen from Figs. 3 and 4, the predictions of both models fit the experimental data reasonably well. The experimental curves depart from the straight line, below 300°C, because of the appearance of a series step, connected with the low-temperature branch, which has not been taken into account up to now. This effect is more pronounced at the lowest temperatures and for high frequencies. In a next step, the contribution of such a series step was included by fitting the values predicted by Eq. (15) to our experimental data. By comparing the temperatures at which the experimental phase lag, ϕ, becomes 90° ($\tan\phi = \infty$) with those predicted theoretically, the preexponential and activation energy

for the series step can be estimated as: $A_3^o = 10^4 \pm 1$ sec^{-1}, and $E_3 = 2 \pm 1$ kcal/mole. We do not know what the series step can be, although the order of magnitude of the preexponential could correspond to that of a pseudo-first-order one, like that corresponding to branch 1 (the low-temperature branch in the parallel models). It is difficult, however, to rationalize how the two second-order processes could be connected in series. With the values indicated above for A_3^o and E_3, the curves plotted as broken lines in Fig. 4 were calculated.

For the amplitude curves, the two parallel models I and II predict a very similar behaviour, and only the values of r computed for model II are shown as solid lines in Fig. 3. For the lowest frequencies, there is a disagreement with the predicted values at low temperatures. The inclusion of the series step does not improve the situation appreciably. The strong decrease in the amplitude at the lowest temperatures observed expreimentally may be due to contamination of the surface since the cooling rate there was very slow. The contaminant was probably CO, the main component in the ambient. Although the Auger spectrum of the Pt surface at the end of the experiment showed only a very small carbon peak (with a ratio C_{272}/Pt_{237} of $\lesssim 1/6$), it is likely that most of the adsorbed CO may have been desorbed by the incident electron beam by the time the carbon peak was recorded (e-beam energy = 2 KeV, intensity $\simeq$ 20 μA).

4.3. The Pt(111) Crystal Surface

Most of the comments made in the discussion of the data for the stepped crystal can be repeated here. The pseudo-first-order preexponential A_1 and the activation energy E_1 measured directly from the experimental

plots, corresponding to the low-temperature branch, are, in this case: $A_1 = (2.7 \pm 1) \times 10^5$ sec^{-1}, and $E_1 = 15.6 \pm 0.5$ kcal/mole. By the same arguments used in the case of the Pt(332) crystal, the value of the pre-exponential factor is what should be expected for a second-order process, since for the same beam intensity we deduce $A_1^o \simeq 10^{-2}$ cm^2/sec. The value of A_1 (and hence of A_1^o) is somewhat larger for Pt(111) than for Pt(332), and the activation energy also is larger by approximately 2.5 kcal/mole for the flat crystal. However, the measured value of E_1 contains a contribution due to the activation barrier for dissociative adsorption which, we believe, is present for the flat (111) crystal. The major difference when compared with the stepped crystal appears in the high-temperature region of the r vs. 1/T data. In this region, the phase lag contributed by both the high- and low-temperature branches is small, such that $r \simeq 2\sigma$. In the case of the Pt(332) crystal, there is a flat region as a consequence of the constant value of σ. This, in turn, is a consequence of the non-activated dissociative adsorption of H_2. The inclined straight line observed for the Pt(111) surface means that σ can be written as:

$$\sigma = \sigma_o \cdot \exp(-D/RT) \qquad (16)$$

as expected in the case of an activated adsorption. The values of D and σ_o can be measured directly from the slope and intercept at the origin in the high-temperature region of the ln r vs. 1/T curves. The measured values are: D = 1.5 kcal/mole and $\sigma_o = 0.28$. From Eqs. (14) and (16) we see that the measured slope in the tanϕ data gives $E_1 = E_1' + D$. We then deduce that the activation energy for H-H recombination in the absence of the mentioned

barrier for dissociative adsorption, D, would be of approximately $E_1' \simeq 14$ kcal/mole, a value which is only slightly larger than that corresponding to the stepped crystal (13 kcal/mole).

The calculated curves shown in Figs. 5 and 6 have been computed by the same procedure as for the Pt(332) crystal. The same uncertainty is present for the values of A_2 and E_2 (high-temperature branch) as that described for the stepped surface. The values used in the calculations are (for model II only): $A_2^o = 10^{12}$ sec^{-1} and $E_2 = 27$ kcal/mole. Here also the best fit is for $p \simeq 1/4$.

4.4. The Activated Adsorption of H_2 on Pt(111)

The results of studies in this laboratory that have been previously reported (6, 7) must be included in the discussion of the activation energy barrier for adsorption of hydrogen on the Pt(111) surface, deduced from the dependence of the sticking coefficient on crystal temperature, D = 1.5 kcal/mole. In our previous study of the production of HD as a function of the angle of incidence of the reactant beam (6, 7), the reaction probability was found to be highest at normal incidence. Shown in Fig. 12 are the previously published data as well as our new measurements. Another result of our previous work is that the dependence of the H_2-D_2 reaction probability on the temperature of the reactant beam put an upper limit of 0.5 kcal/mole on the activation energy barrier for adsorption.

The fraction of reactant molecules that have a component of velocity perpendicular to the surface large enough to overcome the barrier, D, can be calculated. For our Maxwellian beam, this fraction is $\exp(-D/RT\cos^2\theta)$

$$\sigma = \sigma_0 \exp(-D/RT\cos^2\theta) \qquad (17)$$

where θ is the angle of incidence of the molecular beam. The angle of incidence dependence predicted by Eq. (17) for various values of the parameter, D, are shown as continuous lines in Fig. 12. The values of D that best fit the experimental data are all below 0.5 kcal/mole, in agreement with the upper limit for D deduced from the beam temperature dependence of the amplitude of the HD product.

There appears, then, to be a conflict between the values of D deduced from the crystal temperature experiments, 1.5 kcal/mole and the beam angle of incidence and beam temperature experiments, $D \lesssim 0.5$ kcal/mole. It is not clear, however, if these two types of experiments should give exactly the same result. The incident H_2 molecules can be divided into two classes, the molecules that have enough kinetic energy to overcome the barrier D and those that do not. The molecules in the first class will be able to dissociate directly upon impact. Those of the second class may still adsorb in a precursor state and later, by adsorbing energy from the solid, may dissociate. In order to compute the contribution of these two types of molecules to the total sticking coefficient, the steric factors for the energetic molecules, the condensation coefficient into the precursor state,and its dependence on angle of incidence must be known.

4.5. The Adsorption of H_2 on Pt(332)

In the case of the Pt(332) crystal, the beam temperature experiments reported in reference 7 also put an upper limit of0.5 kcal/mole for any barrier for dissociation, for any of the incident beam directions. The

high-temperature region of the r vs. 1/T data (see Fig. 3) indicates that there is no activation barrier for dissociation, in agreement with the beam-temperature experiment.

There is one important consequence of these results. The terrace region, of 6 atoms width and (111) orientation, does not behave like the infinite (111) plane. The adsorption is activated on the (111) surface but not on the terraces of the stepped crystal. This important result indicates that the presence of steps not only introduces new types of sites on the surface (those associated with the step edges), but also modifies the H-H bond breaking properties of the (111) sites on the terraces.

4.6. Angular Distribution of HD from the Stepped Pt(332) Crystal Surface

The angular distributions shown in Fig. 9, for both azimuthal angles, appear to be closer to a $\cos^2\Omega$ than to a $\cos\Omega$ function. Since a thermally accomodated gas should desorb from a surface in a cosine distribution, and there is no activation energy for adsorption in this stepped crystal, the observed distributions may indicate that the HD product desorbs at higher temperature than that of the Pt substrate (14). That, in turn, may be interpreted as a result of an exothermic reaction, followed by a very short residence time in the molecular state, such that the HD molecule has no time to become thermalized with the substrate. This result could be checked by measuring the velocity distribution of the emitted HD molecules. This type of experiment has been performed for HD molecules desorbing with a $\cos^{3.5}\theta$ angular distribution from a 50% sulfur covered nickel surface (15). In this experiment, it was shown that the desorbed molecules have a velocity distribution which corresponds to a temperature higher than that of the Ni substrate.

4.7. Comparison with the Results of Other Authors

This study of the H_2-D_2 exchange reaction represents a major effort to clarify and extend the earlier work in our laboratory on the Pt(111) and the stepped Pt(997) and Pt(553) surfaces (1, 2). The use of the integral mode of detection and lower modulation frequencies has improved the overall quality of the experimental data. More detailed structure in the tanϕ vs. 1/T curves below $\sim$800°C has been observed due to the increased number of data points obtained. In the previous investigation (2), the phase lag vs 1/T curves showed a minimum near $10^3/T \sim 1.3$. At higher temperatures the phase lag increased again up to the highest temperature investigated. We have also observed such a phase reversal, but at somewhat higher temperatures. However, since the phase lags approach zero at the minimum, our results show considerable scatter above $\sim 10^3/T = 1.3$. The phase reversal observed in the earlier study was attributed to a branch mechanism (2, 16). An alternative explanation may be that at these high surface temperatures, dissolution of hydrogen into the bulk may increase the residence time at the crystal, resulting in an increase in the phase lag of the product HD. We have also observed a decrease in the apparent reaction probability accompanying the increasing phase lag, which could be attributed to a decrease in the surface concentration of H and D atoms due to bulk diffusion.

Christmann et al. (4, 5), in their study of the H_2-D_2 exchange reaction on the Pt(111) and stepped Pt(997) surfaces, have found an activation energy of 2.5 kcal/mole below 300°C for both crystals. These results were obtained by thermal desorption, a zero modulation frequency technique, and therefore should be compared to the prediction of our models at f = 0,

i.e., the slope of an Arrhenius plot of the sticking coefficient. For the Pt(111) surface, we find an activation energy of 1.5 kcal/mole, which is somewhat smaller than that measured by Christmann et al. (4, 5), but larger than that reported by Lu and Rye[3], 1.2 kcal/mole. On the stepped Pt(332), no activation energy for dissociative adsorption was observed. It is not clear, however, that the results for the Pt(332) crystal should be similar to those obtained for the Pt(997) surface, since for the stepped crystal used in our study, the density of steps is almost a factor of two larger. One question that remains open is what the width of the terrace region should be for the appearance of activated adsorption, as for the infinite (111) plane.

Our results for activated adsorption of hydrogen on Pt(111) appear to be in good agreement with those reported by Smith et al. (17), an activation barrier of $\sim$1.8 kcal/mole for the adsorption of D_2 on Pt(111).

The existence of two or more types of sites for hydrogen adsorption on many platinum single crystal surfaces have been observed by thermal desorption (4, 5, 11 and 12). For Pt(111) the investigations of various authors indicate that one (3, 18), two (4, 12) or three (11) sites are present on the surface. Two studies have compared hydrogen adsorption on the flat (111) to stepped (111) surfaces (Pt(S)-[9(111)x(111)][5] and Pt(S)-[6(111)x(111)][12]). In both cases, the two adsorption sites that were found on the flat (111) surfaces were also observed on the stepped (111) surface, as well as a third higher energy site. Our results indicate, on both the flat (111) and stepped (111) surface, that at least two sites are present which control the recombination reaction simultaneously at high temperatures.

5. Conclusions

(1) The adsorption and dissociation of H_2 on Pt(111) is an activated process. Two different values have been obtained for the height of the barrier depending on the type of experiment: 1.5 kcal/mole from the dependence of the reaction probability for H_2-D_2 exchange on the crystal temperature, and $\lesssim$0.5 kcal/mole from the production of HD as a function of the temperature (velocity) and angle of incidence of the reactant beam.

(2) The adsorption and dissociation of H_2 on the stepped Pt(332) crystal requires no activation energy. The adsorbed molecules have a diffusion length of less than 6 atomic distances on the terraces, at least for crystal temperatures in the range 200-800°C.

(3) After dissociative adsorption, the recombination and desorption of H_2, HD and D_2 follows a similar mechanism in both the flat and the stepped crystals. The reaction channel that is operative in the whole temperature range studied, 25-800°C, and accounts for the formation of about 75% of the HD products, has an activation energy and a pseudo-first-order preexponential factor of E_1 = 13.0 ±0.4 kcal/mole and A_1 =(8 ± 3)x 10^4 sec^{-1} for the stepped Pt(332) crystal and E_1 = 15.6 ±0.5 kcal/mole and A_1 = (2.7±1) x 10^5 sec^{-1} for the Pt(111) crystal. Although the kinetic parameters could not be accurately determined, two other reaction channels were identified, one acting in parallel with the first channel in the temperature range 300-800°C, and another in series with the first channel from 25-300°C.

(4) The sites of the (111) terraces of the stepped Pt(332) crystal do not behave like those of the infinite (111) plane in that the dissociation of H_2 is not activated on the (111) terraces of the stepped surface.

Acknowledgements

The authors gratefully acknowledge the National Science Foundation for their support of this work.

Work supported in part by the U. S. Department of Energy.

References

1. S. L. Bernasek, W. J. Siekhaus and G. A. Somorjai, Phys. Rev. Lett. 30, 1202 (1973).
2. S. L. Bernasek and G. A. Somorjai, J. Chem. Phys. 62, 3149 (1975).
3. K. E. Lu and R. R. Rye, Surface Sci. 45, 677 (1974).
4. K. Christmann, G. Ertl and T. Pignet, Surface Sci. 54, 365 (1976).
5. K. Christmann and G. Ertl, Surface Sci. 60, 365 (1976).
6. R. J. Gale, M. Salmerón and G. A. Somorjai, Phys. Rev. Lett. 38, 1027 (1977).
7. M. Salmerón, R. J. Gale and G. A. Somorjai, J. Chem. Phys. 67, 5324 (1977).
8. R. H. Jones, D. R. Olander, W. J. Sickhaus and J. A. Schwarz, J. Vac. Sci. Technol. 9, 1429 (1972).
9. J. A. Schwarz and R. J. Madix, Surface Sci. 46, 317 (1974).
10. D. R. Olander and A. Ullman, Int. J. Chem. Kin. VIII, 625 (1976).
11. R. W. McCabe and L. D. Schmidt, Surface Sci. 65, 189 (1977).
12. D. M. Collins and W. E. Spicer, Surface Sci. 69, 85 (1977).
13. R. C. Baetzold and G. A. Somorjai, J. Catal. 45, 94 (1976).
14. F. O. Goodman, Surface Sci. 30, 525 (1972).
15. G. Comsa, R. David and K. D. Rendulic, Phys. Rev. Lett. 38, 775 (1977).
16. I. E. Wachs and R. J. Madix, Surface Sci. 58, 590 (1976).
17. J. N. Smith, Jr. and R. L. Palmer, J. Chem. Phys. 56, 13 (1972).
18. B. E. Nieuwenhuys, Surface Sci. 59, 430 (1976).

Figure Captions

Fig. 1. Arrhenius plots of the experimental parameters, the amplitude, r, and the tangent of the phase lag, ϕ, predicted by several reaction models. The form of the amplitude , r, vs. 1/T curves is similar for the three general mechanisms treated, so is shown only in (A) for a single step reaction (first or second order). The variation in the tangent of the phase lag, ϕ, as a function of 1/T is strikingly different for these mechanisms, as shown in (B) for a single step reaction (first or second order), (C) for a branched mechanism, with two reaction paths operating in parallel, and (D) for two reaction channels acting in series.

Fig. 2. HD production on a Pt(332) crystal at 800°C, as a function of the position of the mixed H_2-D_2 beam on the surface, incident at the macroscopic surface normal. The three curves A, B and C are for different mechanical polishing and chemical etching treatments prior to mounting the crystal. In particular, curve A demonstrates the effect of spot-weld damage on the edges of the crystal.

Fig. 3. Arrhenius plots of the amplitude of the HD product at several beam modulation frequencies on the Pt(332) surface. As depicted in the insert, the angle of incidence of the mixed H_2-D_2 beam is $\theta = 45^{o}$, measured from the macroscopic surface normal. The reactant beam impinges perpendicular to the step edges into the open side. Shown as continuous lines are the calculated curves for reaction model II.

Fig. 4. Arrhenius plots of the absolute value of the tangent of the phase lag, ϕ, for the HD product on the Pt(332) surface at several beam modulation frequencies. As depicted in the insert, the angle of incidence of the mixed H_2-D_2 beam is $\theta = 45^o$, measured from the macroscopic surface normal. The reactant beam impinges perpendicular to the step edges into the open side. The filled circles and squares correspond to negative values of $\tan\phi(\phi>90^o)$. The continuous curves have been computed using reaction model II. The dashed curve (---) around $10^3/T \approx 1.8$ and f = 50 Hz is the prediction of reaction model I. The dashed and dotted curves (-•-•-) were calculated for a series process.

Fig. 5. Arrhenius plots of the amplitude of the HD product on the Pt(111) surface at several beam modulation frequencies. The mixed H_2-D_2 beam impinges normal to the surface. Shown as continuous lines are the predictions of reaction model II.

Fig. 6. Arrhenius plots of the absolute value of the tangent of the phase lag, ϕ, for the HD product on the Pt(111) surface at several beam modulation frequencies. The mixed H_2-D_2 beam impinges normal to the surface. The filled triangles and circles correspond to negative values of $\tan\phi(\phi>90^o)$. Shown as continuous curves are the predictions of reaction model II.

Fig. 7. An example of the hysteresis observed in the phase lag, ϕ, vs. 1/T curves, shown for the Pt(111) surface. The mixed H_2-D_2 beam is incident normal to the surface with a modulation frequency of 50Hz. In general, the phase lag, ϕ, is larger for the heating cycles than for the cooling ones. This effect was present on both the flat (111) and the stepped (332) surfaces.

Fig. 8. The effect of silicon segregation to the Pt(111) surface on the amplitude of the HD product, for several beam modulation frequencies. The mixed H_2-D_2 beam is incident normal to the surface. Shown as a dashed line is the HD amplitude when no silicon is present on the surface, as in Figure 5.

Fig. 9. Angular distribution of the HD product from the Pt(332) surface, measured in the plane defined by the macroscopic surface normal and the incident reactant beam, for two azimuthal angles, Φ. As depicted in the insert, when $\Phi = 90^{o}$, the mixed H_2-D_2 beam impinges perpendicular to the step edges, into the open side (plotted as filled circles). For $\Phi = 0^{o}$, the projection of the incident beam on the surface is parallel to the step edges (plotted as open circles). In both cases, the angle of incidence of the reactant beam is $\theta = 45^{o}$, relative to the macroscopic surface normal. The dashed lines correspond to a cosine dependence on the scattering angle, Ω, and the solid lines to a cosine squared dependence.

Fig. 10. HD production as a function of the angle of incidence, θ, of the mixed H_2-D_2 beam on the Pt(332) surface for several crystal temperatures at 1.8Hz. The beam impinges perpendicular to the step edges, into the open side for positive angles of incidence, as depicted in the insert.

Fig. 11. HD production as a function of the angle of incidence, θ, of the mixed H_2-D_2 beam on the Pt(332) surface at 100°C and 1.8Hz. As depicted in the insert, the reactant beam impinges perpendicular to the step edges. The arrows in the dashed lines indicate the order, in time, in which the measurements were made. A steady decrease in the HD signal is observed, probably due to adsorption of background gases on the surface.

Fig. 12. Variation of the HD amplitude as a function of the angle of incidence, θ, of the mixed H_2-D_2 beam on the Pt(111) surface at 800°C and 10Hz. The continuous curves are the predicted behavior for various values of the activation barrier for adsorption, D, in kcal/mole.

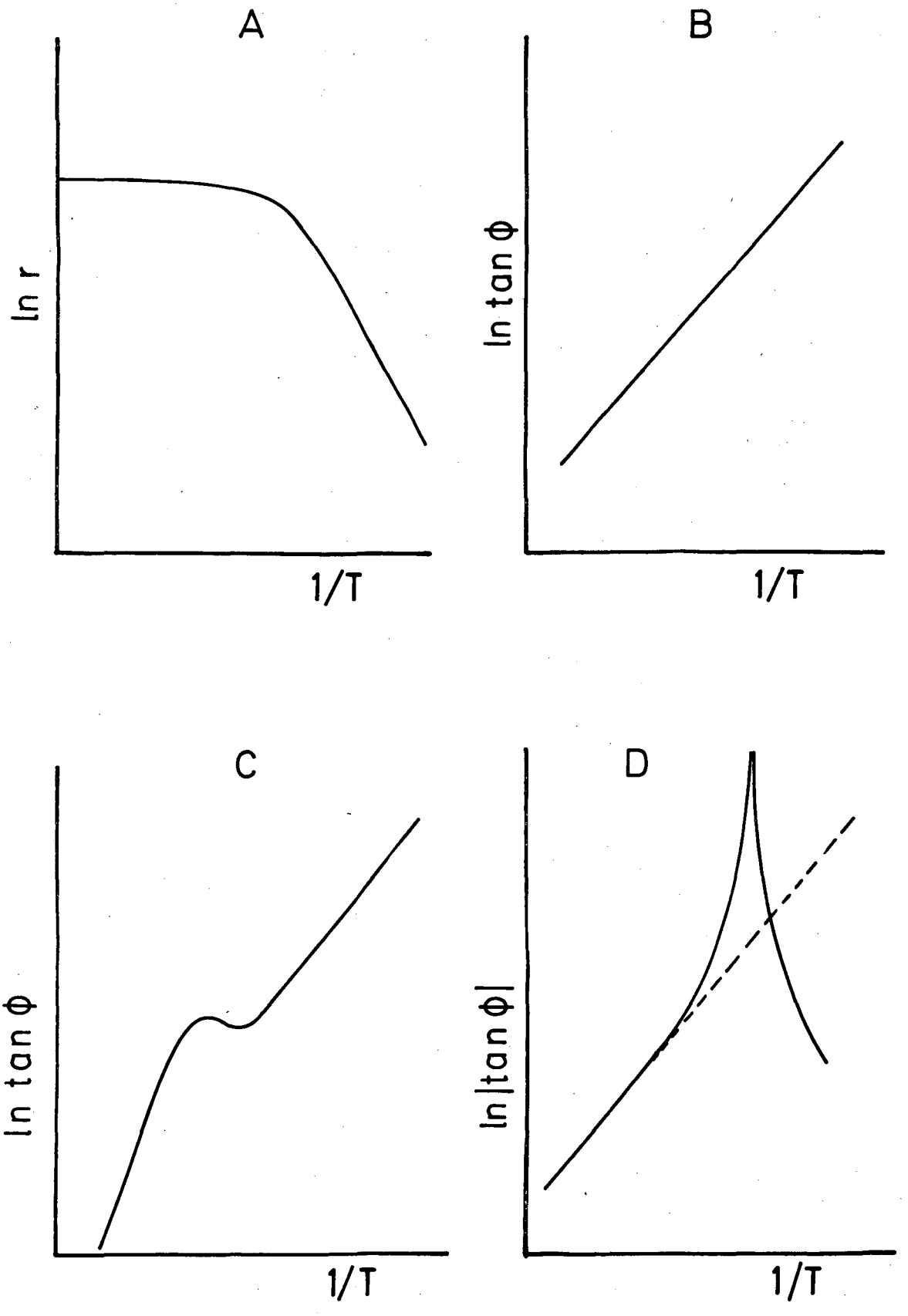

Fig. 1

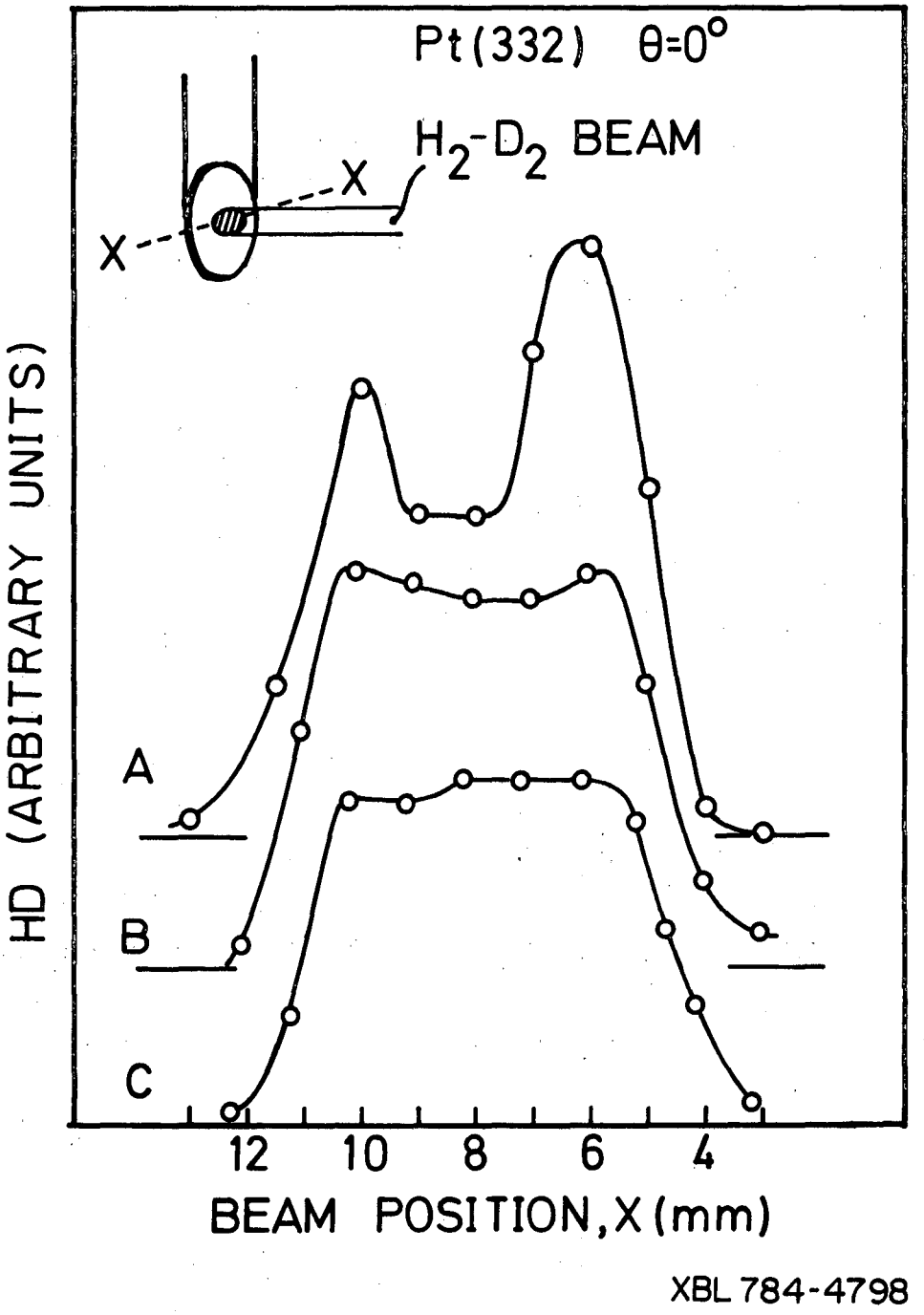
Pt(332) θ=0°
H2-D2 BEAM
X
X
HD (ARBITRARY UNITS)
A
B
C
12
10
8
6
4
BEAM POSITION, X (mm)
XBL 784-4798

Fig. 2

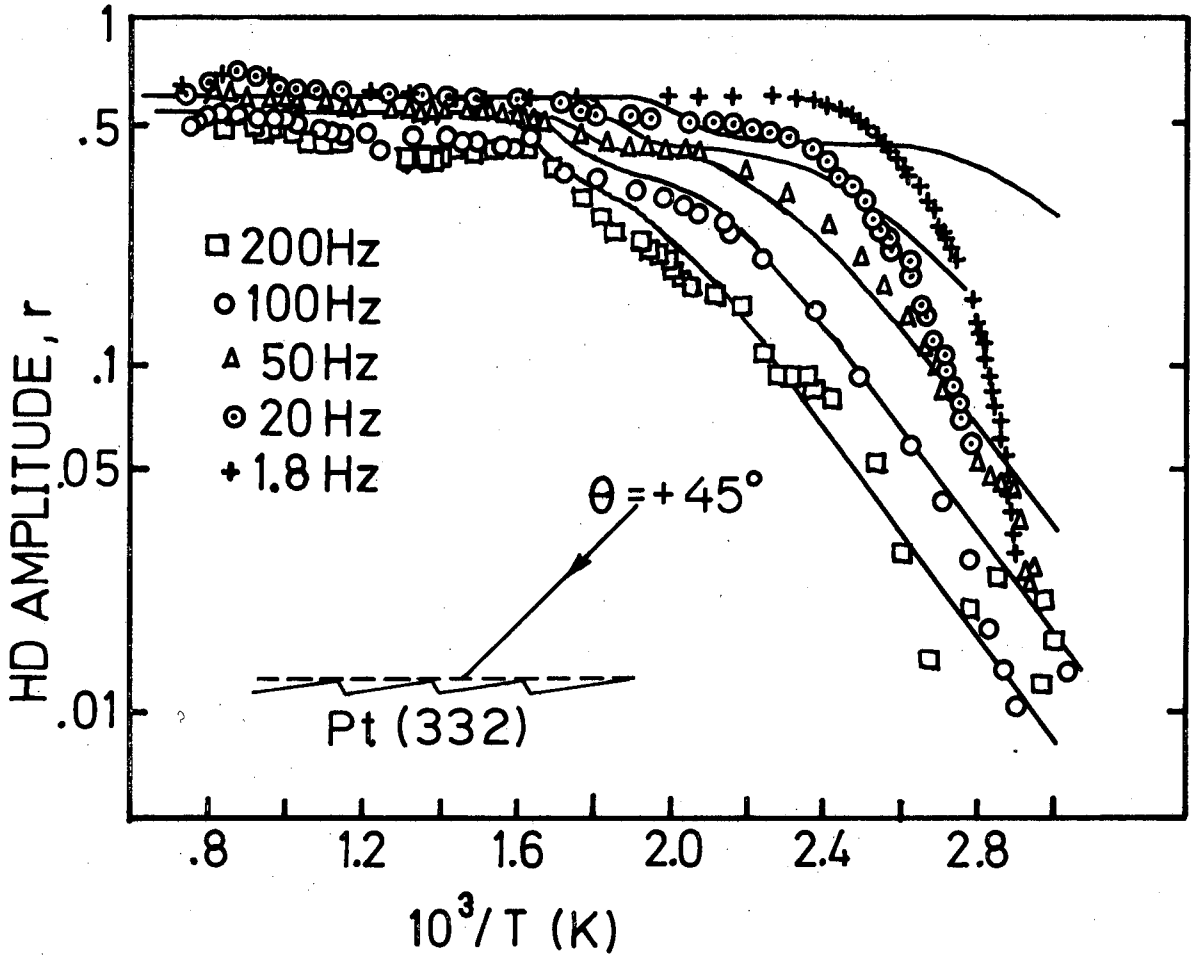
1
.5
.1
.05
.01
HD AMPLITUDE, r
200Hz
100Hz
50Hz
20Hz
1.8 Hz
θ = +45°
Pt (332)
.8
1.2
1.6
2.0
2.4
2.8
10³/T (K)
XBL784-4799

Fig. 3

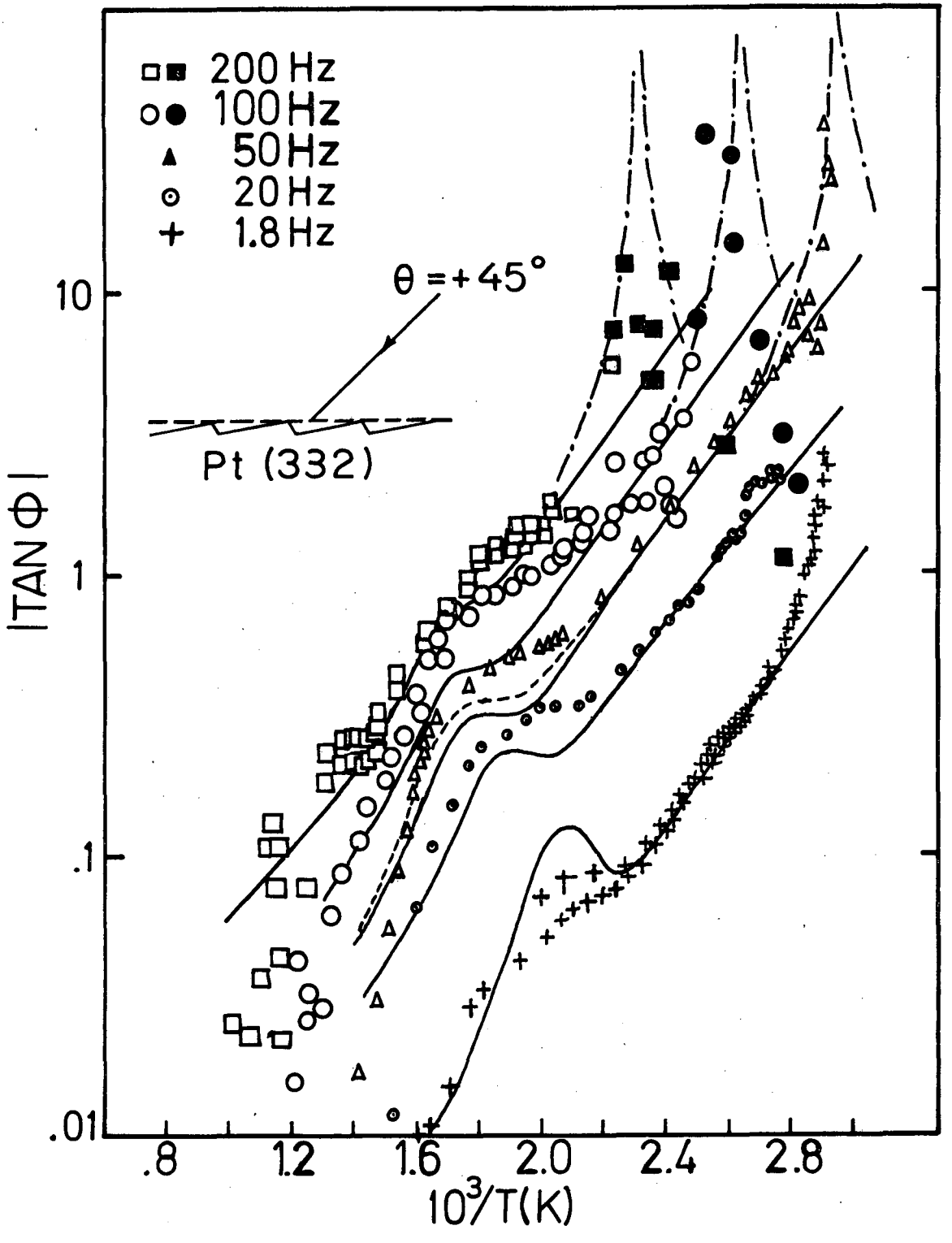

XBL 784-4800

Fig. 4

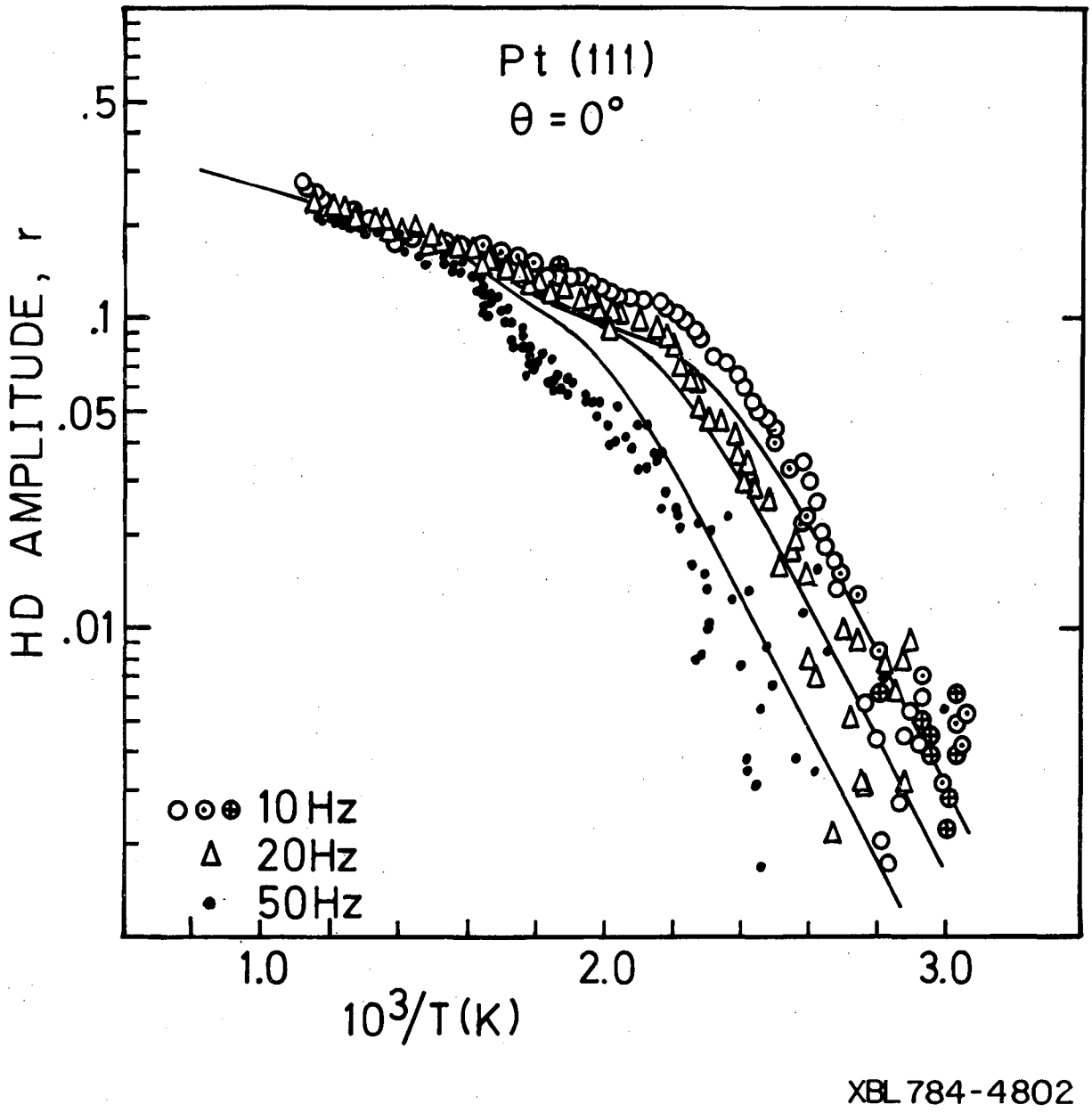
Pt (111)
θ = 0°
HD AMPLITUDE, r
.5
.1
.05
.01
10 Hz
20Hz
50Hz
1.0
2.0
3.0
10³/T(K)
XBL784-4802

Fig. 5

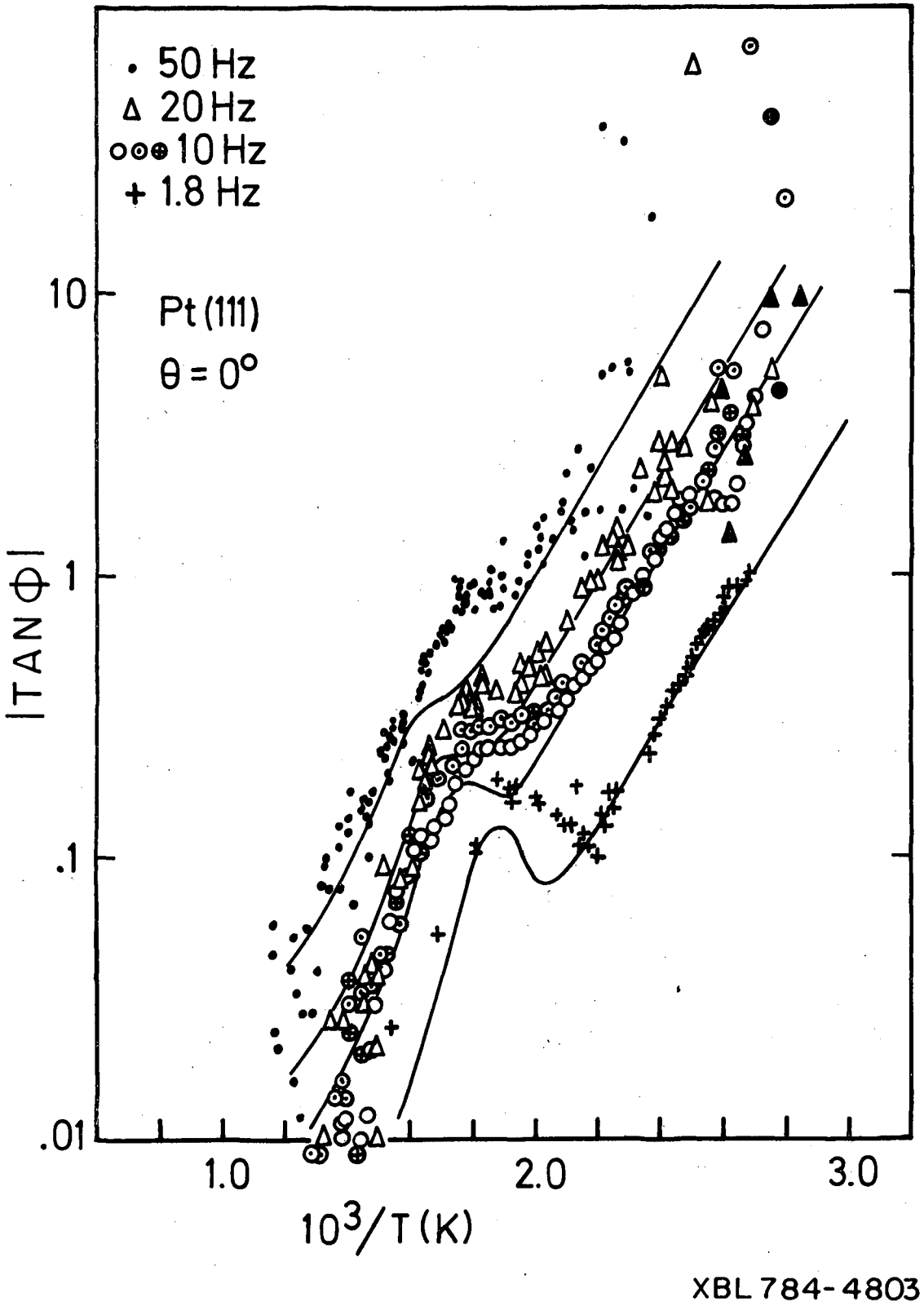
• 50 Hz
Δ 20 Hz
○⊙⊕ 10 Hz
+ 1.8 Hz
Pt (111)
θ = 0°
10
1
.1
.01
|TAN Φ|
1.0
2.0
3.0
10³/T (K)
XBL 784-4803

Fig. 6

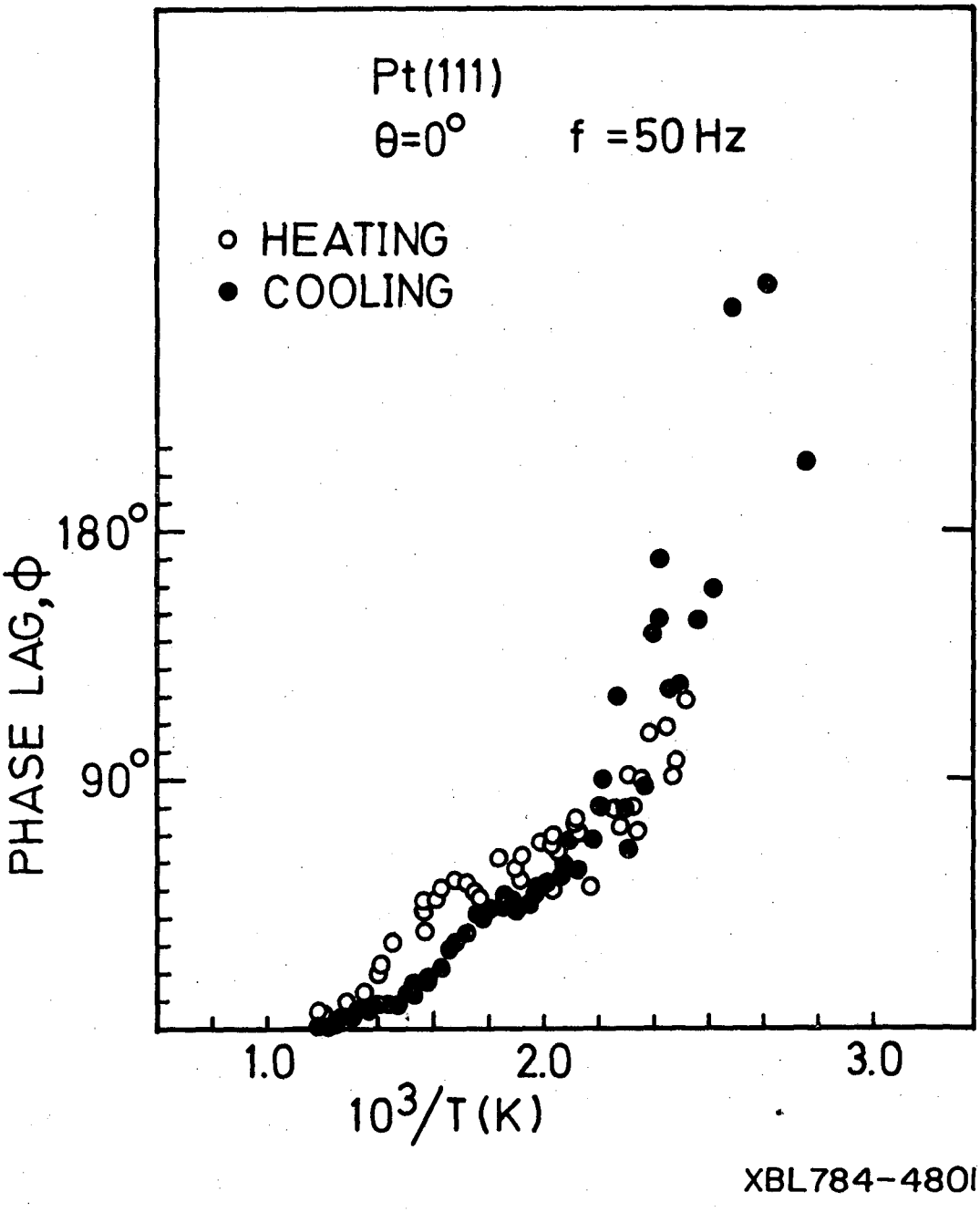
Pt(111)
θ=0°
f =50 Hz
o HEATING
• COOLING
PHASE LAG, Φ
180°
90°
1.0
2.0
3.0
10³/T(K)
XBL784-4801

Fig. 7

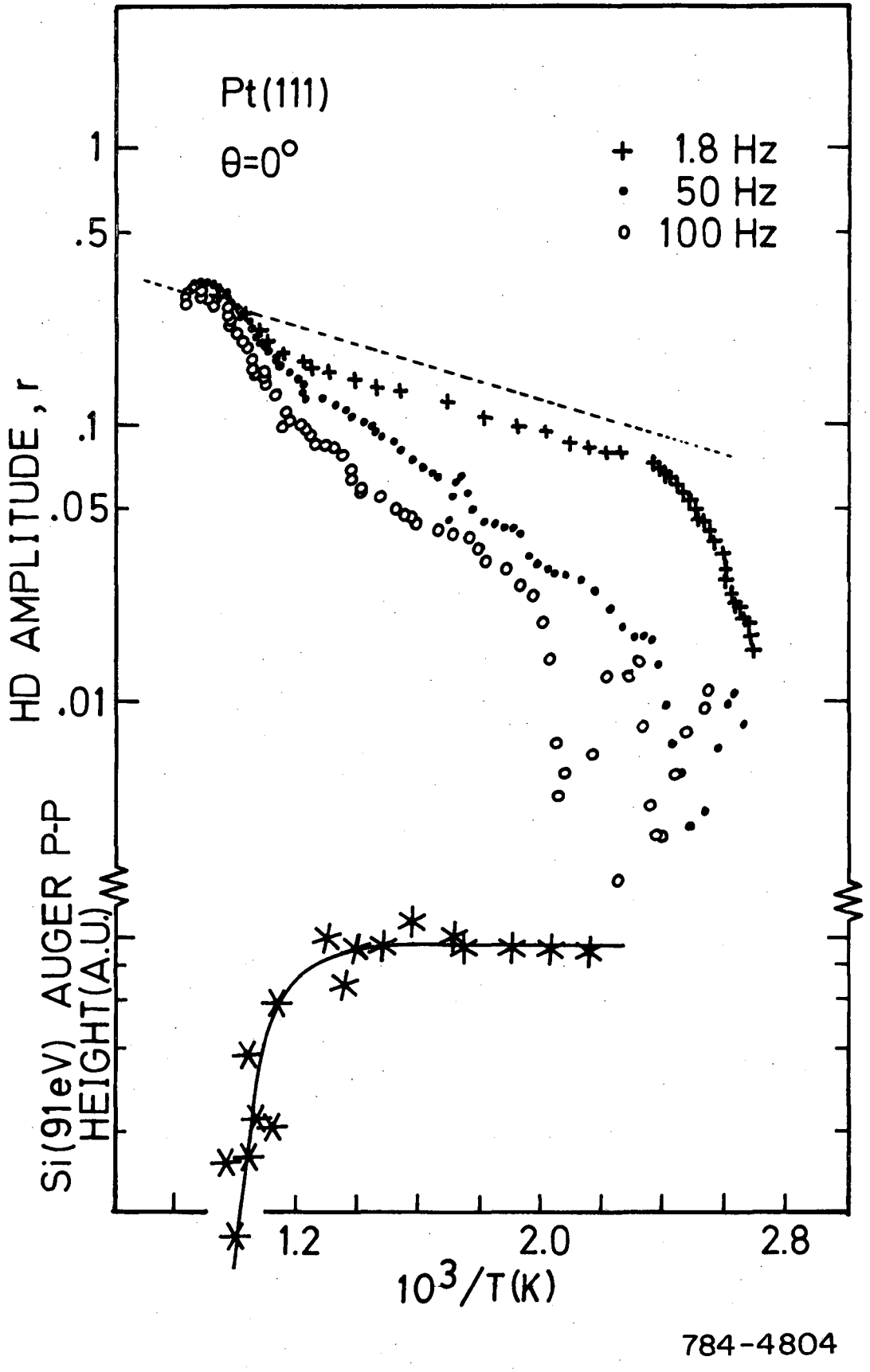
Pt(111)
θ=0°
+ 1.8 Hz
• 50 Hz
o 100 Hz
HD AMPLITUDE, r
1
.5
.1
.05
.01
Si(91eV) AUGER P-P HEIGHT(A.U.)
1.2
2.0
2.8
10³/T(K)
784-4804

Fig. 8

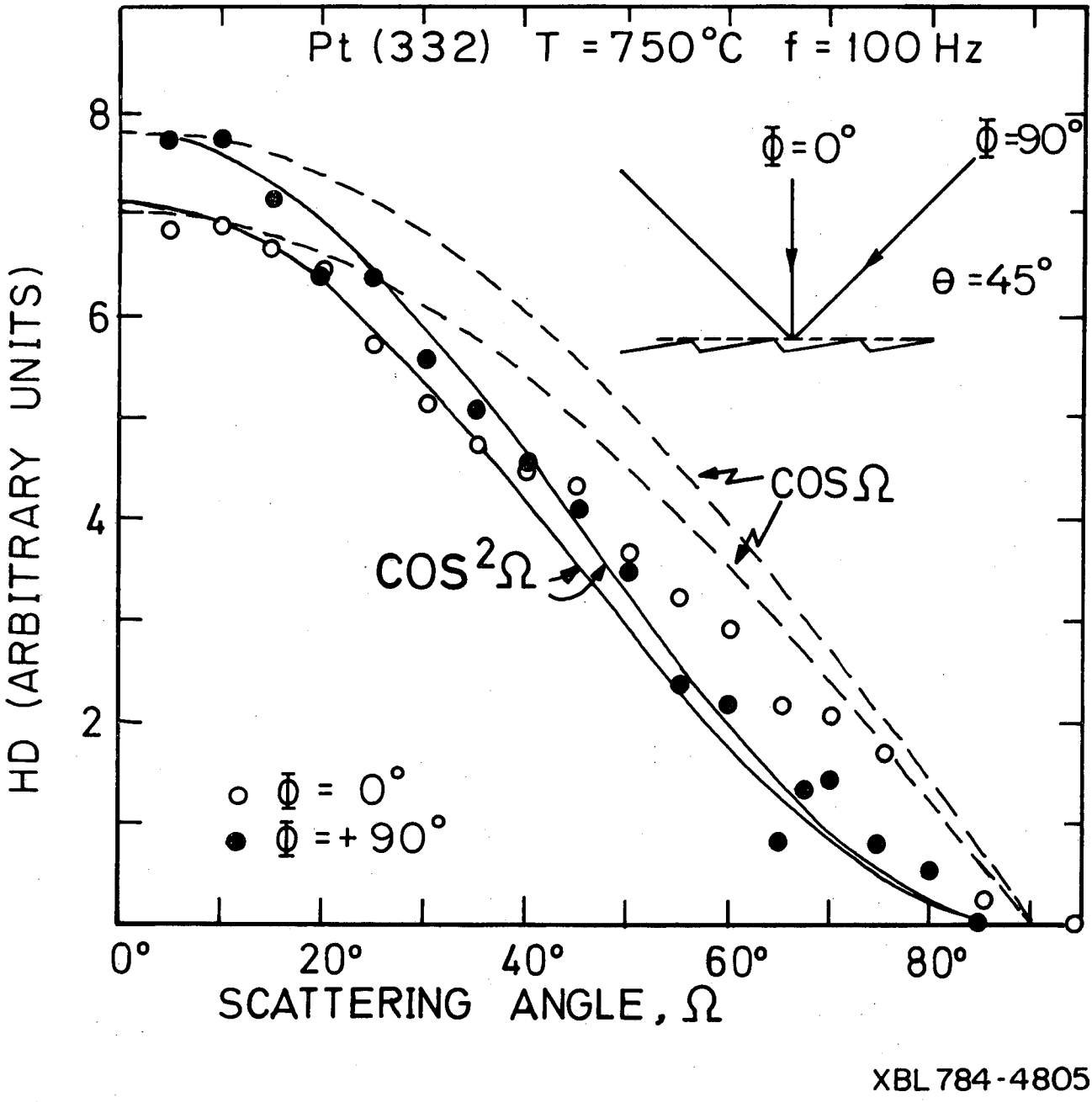
Pt (332) T = 750°C f = 100 Hz
Φ = 0°
Φ = 90°
θ = 45°
COS Ω
COS² Ω
Φ = 0°
Φ = +90°
HD (ARBITRARY UNITS)
SCATTERING ANGLE, Ω
0°
20°
40°
60°
80°
2
4
6
8
XBL 784-4805

Fig. 9

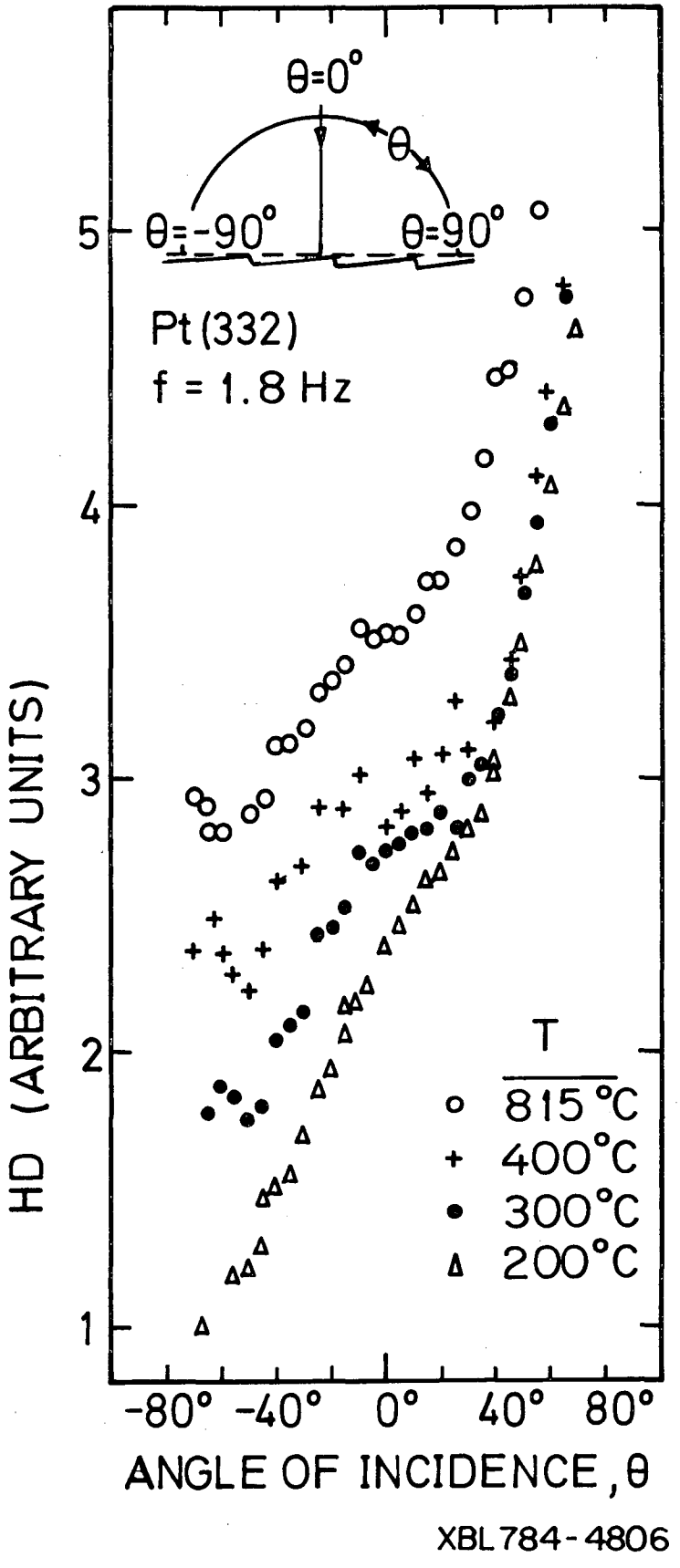
θ=0°
θ
θ=-90°
θ=90°
Pt(332)
f = 1.8 Hz
HD (ARBITRARY UNITS)
5
4
3
2
1
T
815°C
400°C
300°C
200°C
-80° -40° 0° 40° 80°
ANGLE OF INCIDENCE, θ
XBL784-4806

Fig. 10

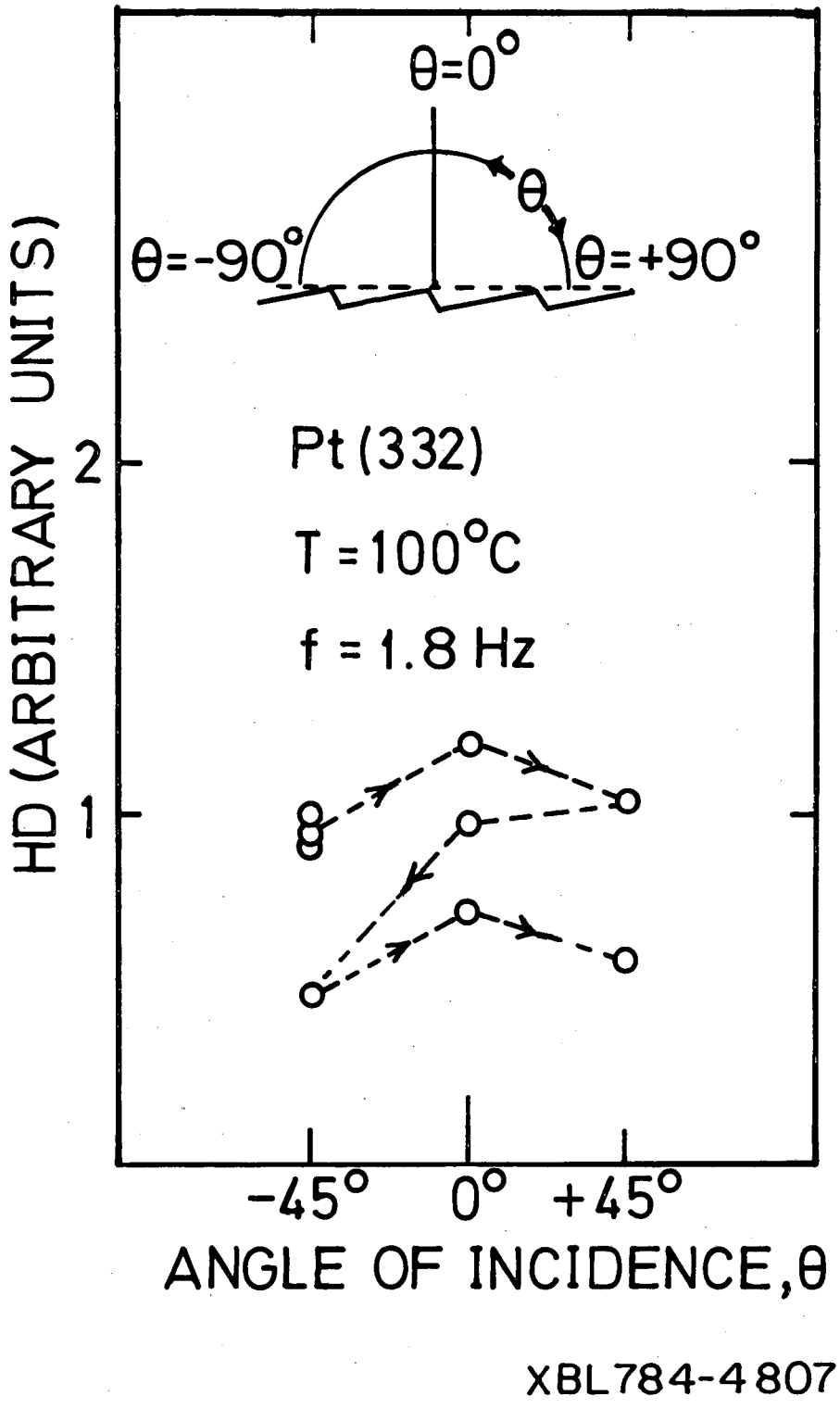
θ=0°
θ
θ=-90°
θ=+90°
Pt(332)
T=100°C
f=1.8 Hz
HD (ARBITRARY UNITS)
2
1
-45°
0°
+45°
ANGLE OF INCIDENCE, θ
XBL784-4807

Fig. 11

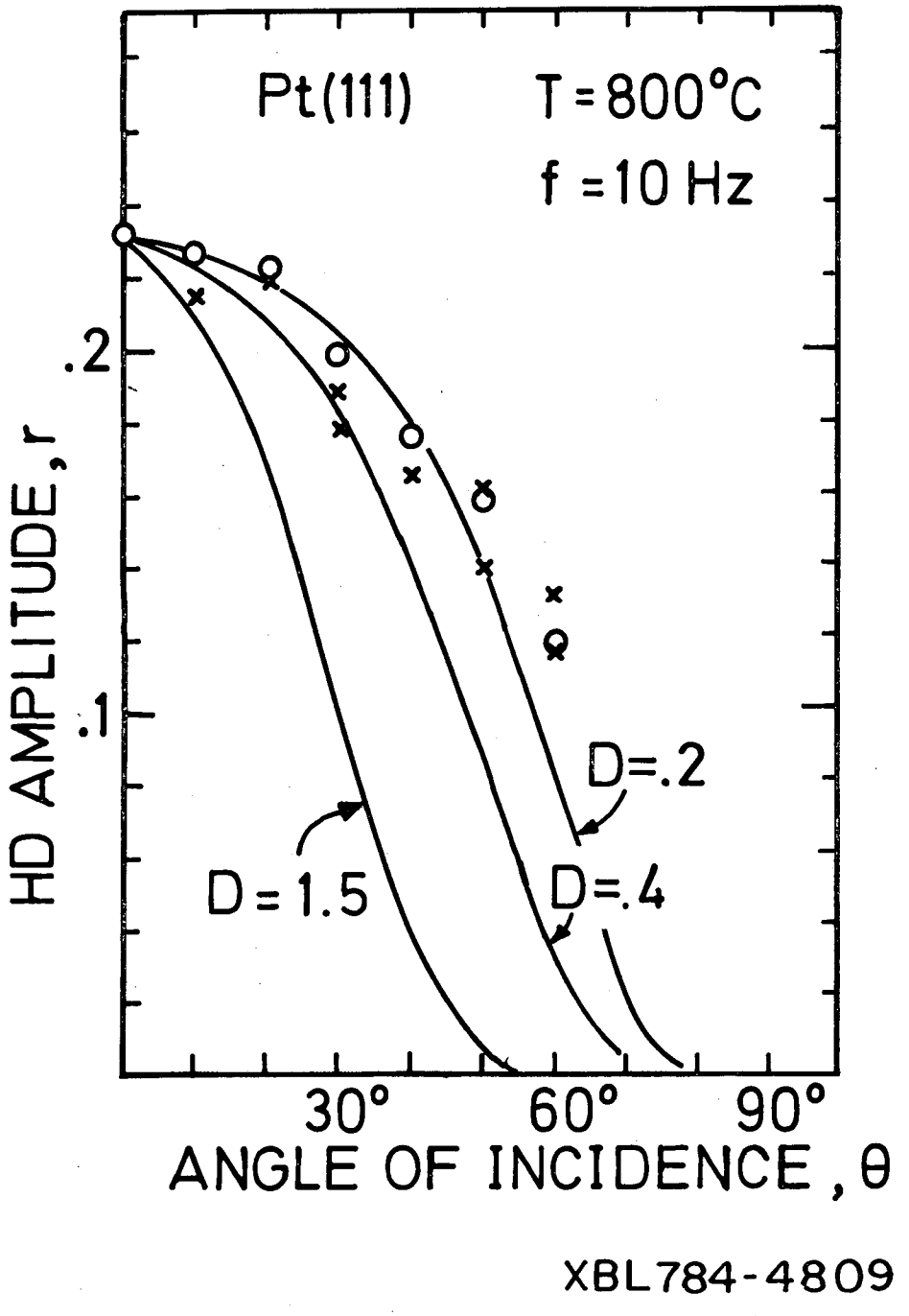
Pt(111)
T = 800°C
f = 10 Hz
.2
.1
HD AMPLITUDE, r
D = 1.5
D=.2
D=.4
30°
60°
90°
ANGLE OF INCIDENCE, θ
XBL784-4809

Fig. 12

TECHNICAL INFORMATION DEPARTMENT
LAWRENCE BERKELEY LABORATORY
UNIVERSITY OF CALIFORNIA
BERKELEY, CALIFORNIA 94720